Splashback Radius of Groups and Galaxies

A Thesis

submitted to
Indian Institute of Science Education and Research Pune
in partial fulfillment of the requirements for the
MS Degree Programme

by

Shree Hari Mittal

Indian Institute of Science Education and Research Pune
Dr. Homi Bhabha Road,
Pashan, Pune 411008, INDIA.

May, 2023

Supervisor: Dr. Susmita Adhikari

Certificate

This is to certify that this dissertation entitled Splashback Radius of Groups and Galaxies towards the partial fulfilment of the MS degree programme at the Indian Institute of Science Education and Research, Pune represents study/work carried out by Shree Hari Mittal at Indian Institute of Science Education and Research under the supervision of Dr. Susmita Adhikari, Assistant Professor, Department of Physics, during the academic year 2022-2023.

Dr. Susmita Adhikari

Committee:

Dr. Susmita Adhikari

This thesis is dedicated to my parents

Declaration

I hereby declare that the matter embodied in the report entitled Splashback Radius of Groups and Galaxies are the results of the work carried out by me at the Department of Physics, Indian Institute of Science Education and Research, Pune, under the supervision of Dr. Susmita Adhikari and the same has not been submitted elsewhere for any other degree.

Shree Hari Mittal

Shree Hari Mittal

Acknowledgments

At the outset I would like to acknowledge those without whose support and company this journey would not have been nearly as enriching.
Firstly, my supervisor, Dr. Susmita Adhikari, for her patience, and constant support. Because of her confidence in me, I find myself continuing on my path to study cosmology. I hope to collaborate with her on projects in the years to come.
My parents, who have supported me, from the time when it was only a dream in the head of a curious teenager. Without their support, I would not be on this path.
My friends and colleagues at IISER, especially Supritha, Archi, and Arijit, who made it feel like home, participated in discussions with me on anything from physics to philosophy and helped me to get away from the work when overwhelmed. I would be amiss to not include friends also on their journey of BS-MS dual degree at IISER, who allowed me space amongst them, and gave opportunity to pursue my non-academic interests
I want to also thank my school friends, who go by the moniker *HnJ*, who even though not at IISER, provided me constant support in all forms, and without their support, I would have not been able to continue my degree, much less finish it.
The list would be incomplete without thanking Dr. Tarun Souradeep, Dr Sunil Mukhi and Dr. Aparna Deshpande, whose guidance and kind words did not let me waiver in my commitment. Dr. Arka Banerjee who has always been open to engage in discussions with me and every student interested in cosmology.
I also want to thank the staff of IISER Pune, who help us students in our hostels, our second home to our professional lives in the academic office, and the technical support.

Abstract

Traditionally, halo radii have been defined based on the spherical over density criterion where the halo radius encloses some over density with respect to the critical or mean density of the universe, leading to definitions such as R_{200c}, R_{200m}, and R_{vir}. Splashback Radius is a proposed, physically motivated definition of halo boundary. It is the radius at which infalling material reaches its first apocenter in a halo. N-body simulations have shown the existence of this feature. Observational evidence of the feature is the next challenge, especially for halos below cluster mass scale. My work includes attempts to bring out this feature for group mass galaxies in the Dark Energy Survey,and study it in different environments of the universe.

Contents

List of Figures

Introduction

Dark Matter halos are one of the fundamental predictions of the standard cosmological model. Density fluctuations at the end of inflationary period of the universe collapse to form the first bound structures. These structures, over time merge to form the massive halos we see in present universe. This is often referred to as the Hierarchical picture of structure formation. These massive halos provide the gravitational well into which baryonic matter falls and clumps to form the galaxies that we can observe. Since dark matter is not directly detectable yet, luminous galaxies are often used as tracers of the underlying dark matter field. By cross- correlating galaxies and clusters, density profiles of the dark matter halos can be created. These profiles contain information about structure formation on smallest scales.

There exist several models to fit the density profile of dark matter halos exist and the first theoretical work was done by cite and cite. These profiles assume a spherical top hat model when predicting halo profiles. Much work has been done to study the inner profile of halos, one famous example being the core-cusp problem. However, the outer edges still remain an unexplored area. In 2014, Diemer and Kratsov [4] proposed a new fitting formula to model the outer profile, alongwith inner profile as well. In this profile, they found a sharp steepening of the profile in outer edges. This was called splashback radius in later work, based on the fitting formula.

Observational studies have detected the splashback feature in cluster size halos, where it is expected to be most prominent. The goal of this project is to detect the feature in clusters and group mass halos. We also know, the formation and evolution of halos is also affected by the environments they live in. This has a direct affect on the outer edges of a halo. To study this effect on splashback radius, the analysis was also done on galaxies in the most under dense and over dense regions of the universe.

The thesis is divided in four chapters. The first one deals with the theoretical basis of splashback radius and the fitting formula for the density profile. The second chapter describes the data used throughout this work, and the various selection cuts made. The third chapter is a discussion on Bayesian Statistics and MCMC. The final chapter is the results and discussion chapter.

Chapter 1

Dark Matter Halos

1.1 Spherical Collapse Model

In an expanding Einstein-de Sitter Universe, dominated by matter,consider a region spherical in shape of radius R_0.[1] The mass enclosed in this region is given by

$$M_0 c^2 = \frac{4}{3}\pi R_0^3 \rho_0 \tag{1.1}$$

where ρ_0 is average matter density at some time in the universe t. If the same sphere is now compressed to a radius r_i, such that $r_i < R_0$ while conserving the mass, the equation becomes

$$Mc^2 = \frac{4}{3}\pi r_i^3 \rho = \frac{4}{3}\pi r_i^3 \rho_0 (1+\delta) \tag{1.2}$$

δ is the over density, which initially is small. Using Newtonian arguments of gravity, the evolution of this spherical region and the over density can be understood. The energy of a particle at some radius r is given as

$$E = \frac{1}{2}\dot{r}^2 - \frac{GM(r)}{r} \tag{1.3}$$

and the equation of motion is

$$\ddot{r} = -\frac{GM(<r)}{r^2} \tag{1.4}$$

[1] This is generally referred as Spherical Top Hat

For any particle such that $r > R_0$, the total mass is M, and $E = 0$,integrating 1.3 gives

$$\begin{aligned} r(t) &= \Lambda t^{\frac{2}{3}} \\ where\ \Lambda &= \left(\frac{9GM}{2}\right)^{\frac{1}{3}} \end{aligned} \tag{1.5}$$

We can use this solution to calculate average density, using 1.1,we get

$$\rho_0 = \frac{3M_0c^2}{4\pi R_0^3} \implies \rho_0 = \frac{c^2}{6\pi G}\frac{1}{t^{\frac{2}{3}}} \tag{1.6}$$

This is the same solution as that of a flat, matter dominated Einstein de Sitter Universe. This is to be expected, since the initial assumption was the same. Now, looking at the more interesting case, of a particle inside the sphere of radius r_i, we have $E < 0$. Integrating 1.4, we get,in parametric form

$$\begin{aligned} r(\theta) &= A(1 - cos(\theta)) \\ t(\theta) &= B(\theta - sin(\theta)) \\ A^3 &= GMB^2 \end{aligned} \tag{1.7}$$

Here, θ is called the development angle, and goes from 0 to 2π. It relates to the conformal time η as

$$\theta = \eta H_0(\Omega_m - 1)^{\frac{1}{2}} \tag{1.8}$$

These equations tell how the spherical region will evolve. For the case when the collapse has just started, that is $r = r_i$, we can take linear case of the equations, which gives

$$r_i \approx \frac{A\theta^2}{2} \text{ and } t_i \approx \frac{B\theta^3}{6} \implies r_i = \frac{A}{2}\left(\frac{6}{B}\right)^{\frac{2}{3}} t_i^{\frac{2}{3}} \tag{1.9}$$

This is actually the same evolution as derived in 1.5. This tells us that the dense region first expands, along with the universe. After some time, it decouples from the expansion and starts collapsing. In fact, it decouples at $\theta = \pi$. This is the first turnaround. We can also solve for the δ evolution as well. From 1.2, we can see the over density will be given as

$$\rho = \frac{3Mc^2}{4\pi r_i^3} \implies \rho = \frac{3Mc^2}{4\pi A^3(1 - cos(\theta))^3} \tag{1.10}$$

We know $1+\delta = \frac{\rho}{\rho_0}$ .From eq. 1.6 and 1.10, we get

$$1+\delta = \frac{9}{2}\frac{(\theta - sin(\theta))^2}{(1-cos(\theta))^3} \tag{1.11}$$

We can again take early time approximation of this equation, by taking terms upto second order in the Taylor series, and putting the value of first turnaround at $\theta = \pi$ we get

$$\delta_{turn} = 1.06 \tag{1.12}$$

Going further along the same logic, we also can get the density contrast when complete collapse happens, that is, at $\theta = 2\pi$, we get

$$\delta_{coll} = 1.69 \tag{1.13}$$

What this means is, where ever in the density field, the density contrast reaches 1.69, it will lead to collapse. This answer is valid only in the linear regime, as the assumptions made to arrive ignore higher order terms. In the spherical collapse model, the overdense region collapses to a point, creating infinite density. However, in reality, due to the angular momentum of the particles, as well mixing between different shells, this singularity is avoided. Eventually, the region settles into equilibrium, to form a dark matter halo. From the Virial Theorem,we know $T = -\frac{1}{2}V$,where T is the total averaged kinetic energy of the system and V is the averaged potential energy. From the 1.3, it's clear that at turnaround, kinetic energy becomes zero, and $V_{turn} = -\frac{GM}{r_{turn}}$. Since energy remains conserved, this is also the energy of the system at late time, when equilibrium is achieved.

$$T_{vir} + V_{vir} = \frac{1}{2}V_{vir} = V_{turn} \implies r_{vir} = \frac{1}{2}r_{turn} \tag{1.14}$$

From the relationship between ρ and r, we can also conclude $\rho_{vir} = 8\rho_{turn}$. The goal is to find density contrast, which from eq. 1.11, after putting $\theta = \pi$ gives

$$\delta_{vir} = 18\pi^2 - 1 \approx 178 \tag{1.15}$$

What we arrived at is one of the most often used definition of a Dark Matter Halo. Irrespective of the initial peak, if a region has 200 times the density compared to that of the background at that redshift, we have a virialised Dark matter halo, and the radius enclosing this region is called the *Virial Radius* or R_{200}. The spherical collapse model is a simplified model. The assumptions of spherical symmetry do not hold in nature. A critical assumption of the model is the constant mass, which also breaks down due to shell mixing. The collapse and evolution of a halo doesn't happen in isolation, and is affected by the surroundings, which the model cannot comment on.

1.2 Density Profile

Dark Matter halos have been studied extensively in the N-body simulations, to understand the physics of halo formation and evolution. Because the interactions are only gravitational in nature but highly non-linear at small scales, numerical simulations have become useful tools to understand halos. One of the remarkable findings from these simulations was the near universality of density profile of dark matter halos, which can be fitted by the NFW profile. It is a two parameter model, and composed of two power laws. The inner regions of the profile have a slope of -1 and the outer profiles have a slope of -3. It is given as

$$\rho(r) = \frac{\rho_s}{\frac{r}{r_s}\left(1 + \frac{r}{r_s}\right)^2} \tag{1.16}$$

ρ_s and r_s are called *scale density* and *scale radius*, and are defined where the slope is -2. The ratio of r/r_s is called the concentration of the halo c_{vir}. The success of NFW and other fitting functions that have since been proposed is noteworthy. However, the main body of work has focused on the inner profiles of these halos. It was observed in simulations that there is a sharp decline in the slope of density profile within a small bin of radius. This could not be explained by NFW or other proposed profiles.
The theoretical understanding of this caustic can be understood by spherical collapse model arguments itself. The radial velocities approach 0 as shells of matter turn around in their orbits at their apocenters. Because of this, subsequent shells of matter pile up against each other forming density caustic. These are narrow, localized regions of enhanced densities. The outer most density caustic in a dark matter halo corresponds to the first apocenter after infall of a shell into the halo potential and acts as the boundary of the virialized region of the halo. Figure shows the caustics and phase-space diagram from simulations.

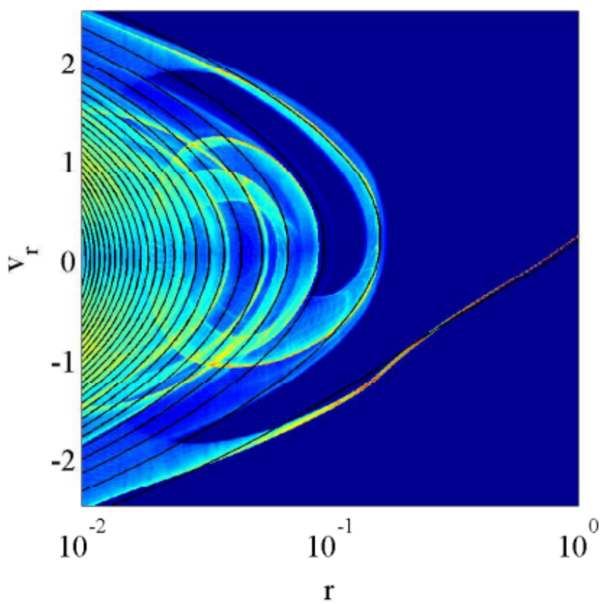

(a) Phase space diagram

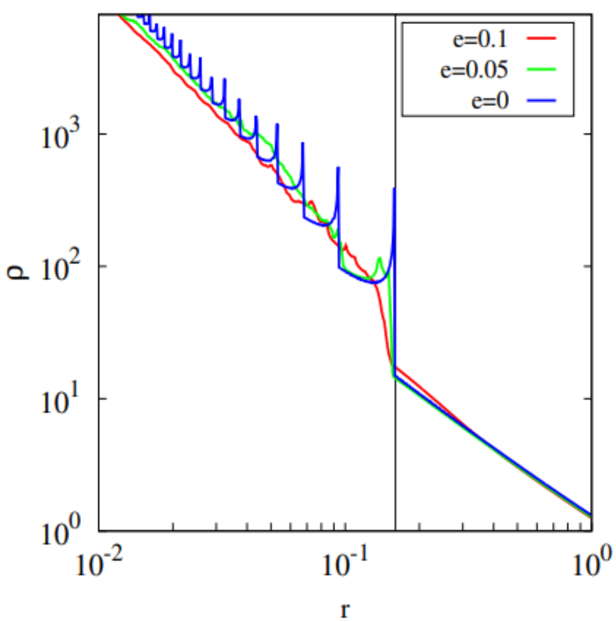

(b) Density Profile

Figure 1.1: Caustics for self-similar halos.The left panel shows the phase space diagram for spherically symmetric collapse (solid black curve) and for 3D collapse with e = 0.05 (color map). The right panel shows density with radius. The black line on the right shows outer most caustic and the splashback radius.[2]

1.2.1 The DK14 Model

In order to fit the density profile and the sharp feature in slope at outskirts of halo, Diemer and Kravtsov proposed a model in 2014. The inner profile is given by Einasto fit, multiplied with a *transition function* The transition term, f_{trans}, captures how the profile steepens around a truncation radius, r_t. The parameters γ and β characterise the steepness of the profile at $r \sim R200m$ and how quickly the slope changes,respectively. The outer profile is given by a power law, with a pivot at r_0. The value of outer mean density and the pivot radius are degenerate with each other, and there

$$\begin{aligned}
\rho(r) &= \rho^{coll}(r) + \rho^{infall}(r) \\
\rho^{coll} &= \rho^{Ein}(r) f_{trans}(r) \\
\rho^{Ein}(r) &= \rho_s \exp\left\{ \left(-\frac{2}{\alpha} \left[\left(\frac{r}{r_s} \right)^{\alpha} - 1 \right] \right) \right\} \\
f_{trans}(r) &= \left[1 + \left(\frac{r}{r_t} \right)^{\beta} \right]^{-\frac{\gamma}{\beta}} \\
\rho^{infall}(r) &= \rho_0 \left(\frac{r}{r_0} \right)^{-S_e}
\end{aligned} \tag{1.17}$$

This is the model used in this work.

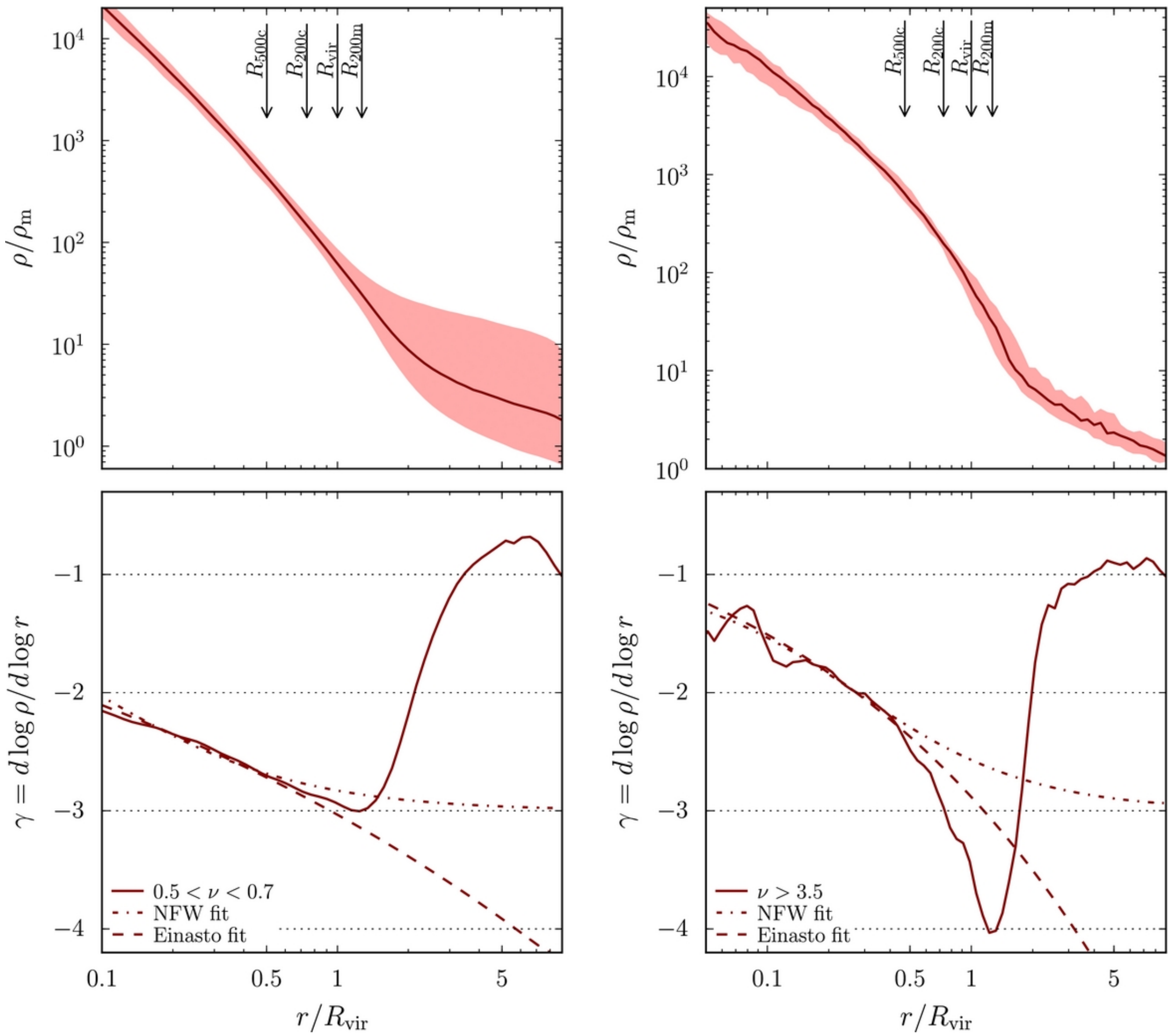

Figure 1.2: The density profile and derivative of log of density with log of radial distance, when fitted with DK14 model. Shaded bands show interval around median that contain 68% of the individual halo profile. The profiles are from N-body simulations, for low mass(left) and high mass(right) halos. The location of splashback is at the minima of the slope. The fit of inner profiles is very close to Einasto/NFW. Various other definitions of radius of halo are also marked.

Chapter 2

Galaxy Groups and Clusters

The visible universe has wide range of astrophysical objects in its catalogue. From planets within our solar systems to galaxies hundreds of thousands of light years away, and everything in between. Galaxy Clusters and groups are one of the largest gravitational bound objects of gas,dust, stars and dark matter. They can be 10 to 1000 times massive than our own galaxy, Milky Way.

This visible universe has been mapped by various surveys over the years. Marking the position of objects in sky over years of exposure has created catalogues of Groups and Clusters. Since Dark Matter is difficult to detect, outside of gravitational lensing, galaxies become the proxy for dark matter distribution.

For the work in this thesis, most of the data used is from Dark Energy Survey(DES)[14]. DES is a survey in the near ultra-violet, optical and near infrared band of EM spectrum. It covered 5000 square degrees of the southern sky, in five bands, $grizY$ (similar to the optical survey SDSS) over a period of six years. It has a depth of nearly $z \approx 1$. The survey used a CCD camera, DECam, specifically built for the survey, mounted over Blanco 4m Cerro Telolo Inter-American Observatory. The catalogues of clusters and galaxies constructed using the survey and used in this work are described in this chapter.

Figure 2.1: Dark Energy Survey Deep Field Image, with many Groups and galaxies. courtesy of NOIRlab

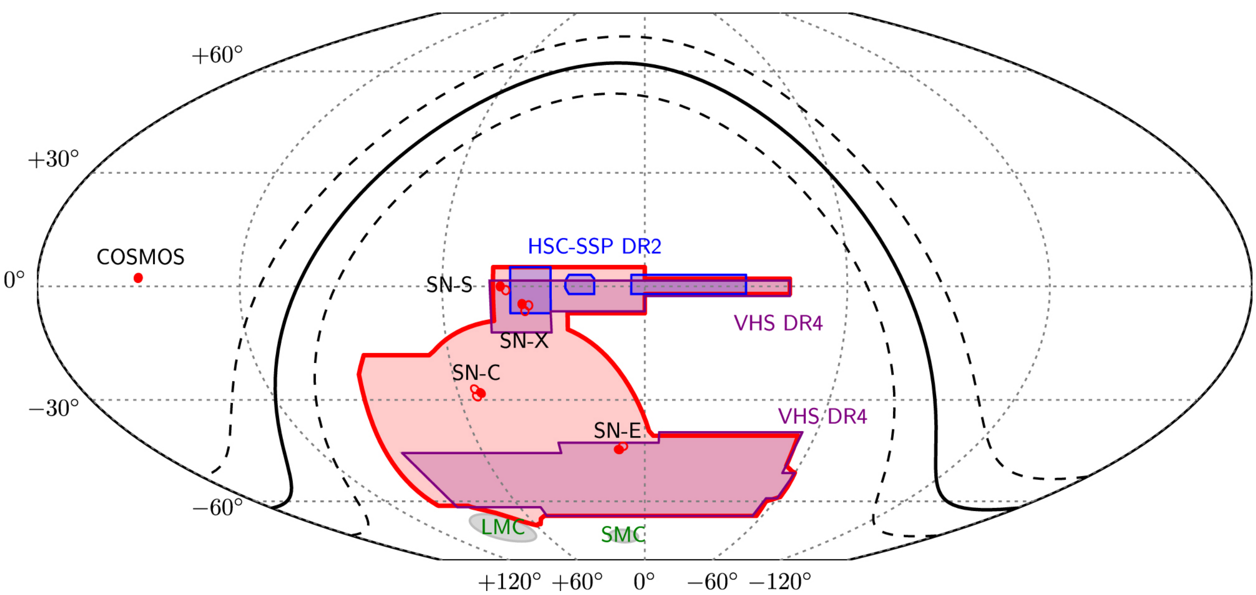

Figure 2.2: Region covered by DES in equatorial coordinates. Also included in this image is Supernova Survey Field("SN"), COSMOS, HSC-SSC DR-2 and VHS-DR4. Filled Red are the deep fields of DES. Solid Black line is Galactic Plane.[6]

2.1 The redMaPPer Galaxy Cluster Catalog

Compared the early days of cosmology, modern day sky surveys are much larger and much deeper. They have millions of objects and therefore, classifying manually these objects becomes herculean task. redMaPPer[11] is one such cluster finding algorithm. It is based on the fact that most of the clusters are made up of old, red galaxies. This helps the algorithm possible candidates in the data. Because the Dark Energy survey is not a spectroscopic survey, redshifts of the galaxies are not available. redMaPPer also gives z estimates. A sequence of galaxies is built, by correlating the magnitude and color of the galaxies. Though there is intrinsic scatter in this relationship, it is calibrated against spectroscopically confirmed galaxies, based on a the simple assumption that member galaxies of a cluster will have the same redshift as the cluster itself. Following this, the redshifts are assigned based on a likelihood method, the principle of which will be discussed in Chapter 3.

The algorithm also gives richness of the clusters, which is analogous to the number of member galaxies in a cluster. The algorithm takes an aperture length, that is, radius around a central that it will look at, and counts satellites around the central. The "central" is defined simply as the brightest galaxy in the over-densities of galaxies. The richness parameter for the algorithm is then defined as sum of probabilities of membership for the satellite galaxies. This richness can then be used to calculate mass of the cluster, using mass-richness relation. For this work, Year 3 redMaPPer catalog is used,which covers the full 5000 square degrees of the survey and is the latest available. Objects are selected between redshift of 0.2 to 0.7, and with richness between 20 to 100. The total number of clusters is $19,121$ with the Redshift and richness cuts. Mean redshift of the sample is 0.47, mean richness 31.22. Random Catalog corresponding to the redMaPPer catalog is also used, to calculate correlation function, discussed in Chapter 4. Previous work has been done on splashback radius of redMaPPer clusters, and the goal of using this catalog was to construct a pipeline that gives consistent results with the previous work.

2.2 The redMaGiC Catalog

The red sequence Matched-filter Galaxy Catalog builds on the red-sequence template of redMaPPer, and identifies Luminous Red Galaxies(LRGs) in the survey[10]. Instead of

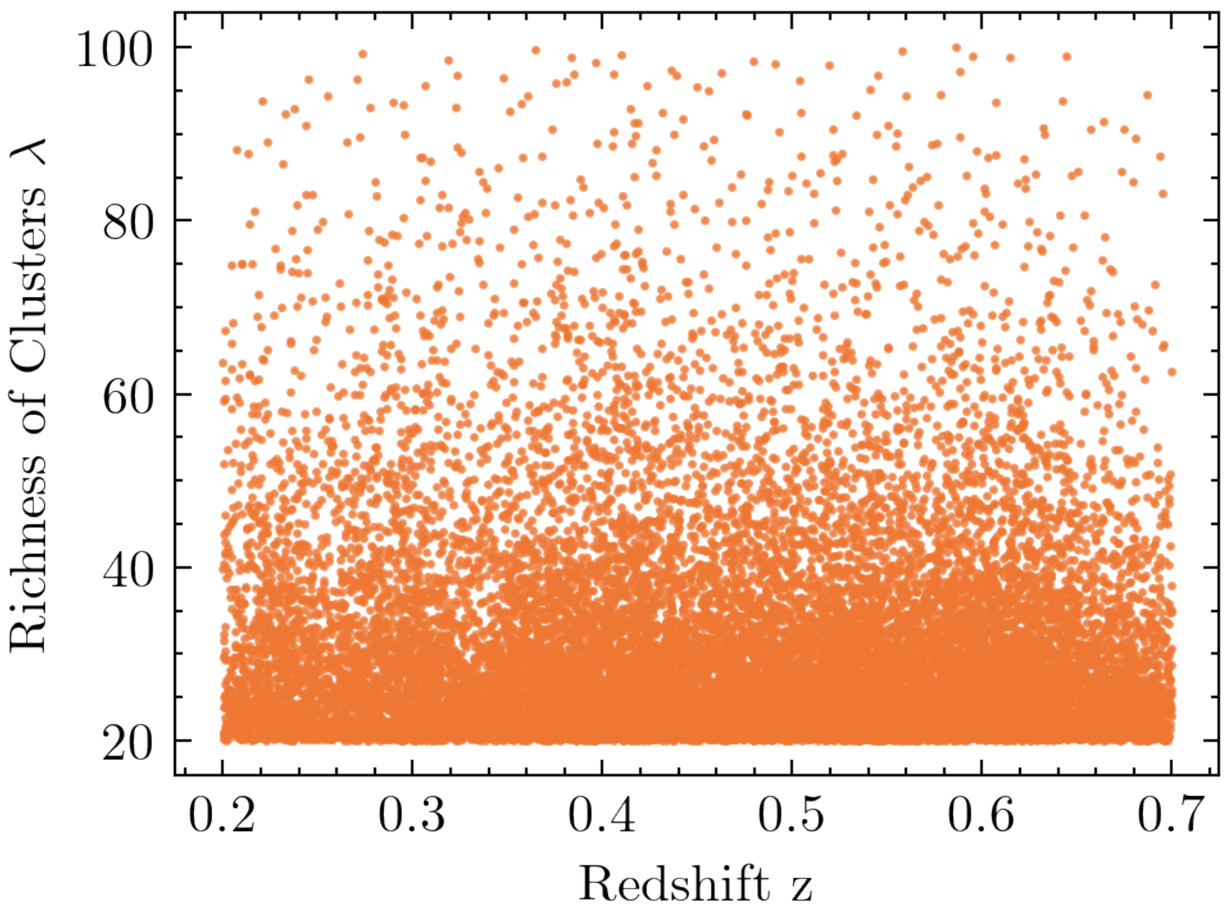

Figure 2.3: Redshift vs Richness distribution of redMaPPer catalog, used in this work.

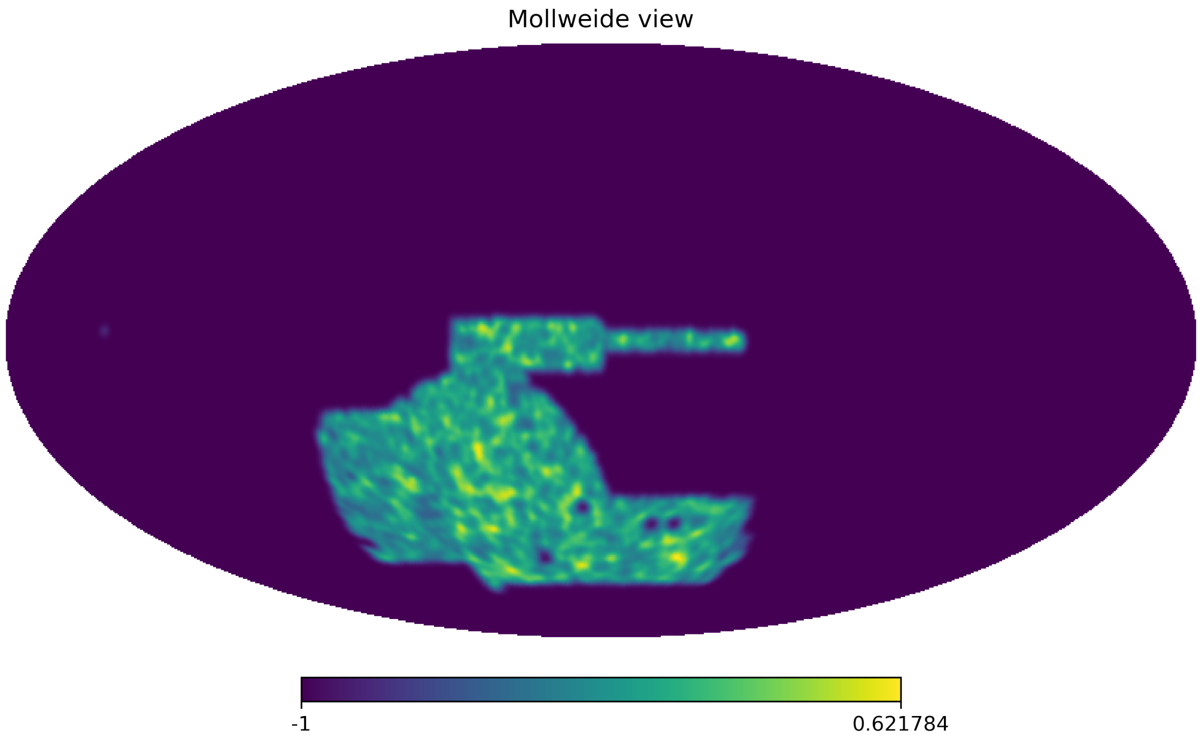

Figure 2.4: Density contrast map of redMaGiC field for $0.45 < z < 0.5$, smoothed over $10 Mpc$.

first applying cuts to select for possible candidates, here, *every* galaxy is fit to the red-sequence template and photo-z estimated. For the computed z, luminosity is calculated. If the galaxy is more luminous than a minimum threshold, and is a good fit to the red-sequence template, the galaxy is included in the catalog. The main advantage of using redMaGiC is very good estimates on redshifts, with low scatter ($\lesssim$ 1.6 per cent) and low bias ($\lesssim$ 0.5 per cent). Random Catalog corresponding to redMaGiC is also used, as in case of redMaPPer to construct correct correlation functions.

2.3 Atacama Cosmology Telescope(ACT) DR5

ACT was a 6 metre, millimeter-wave telescope,located in Atacama Desert, in northern Chile. The telescope detects galaxy clusters through Sunyaev-Zel'dovich(SZ) effect. This work uses Advanced ACTPol cluster sample, as presented in Hilton 2021 [8]. The catalog was

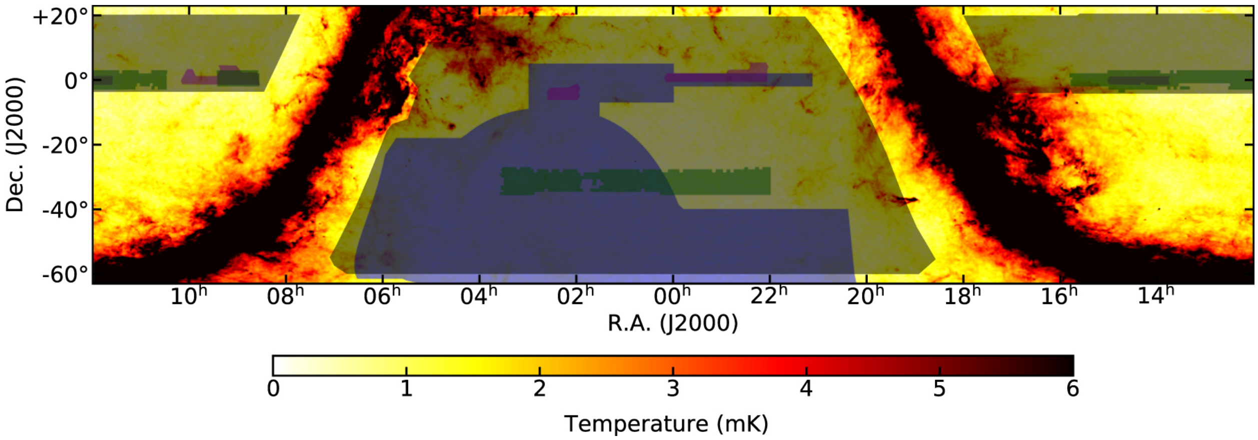

Figure 2.5: Footprint of ACT DR5(in grey), overlaid with Planck 353 GHz map. Other surveys in the map: DES(Blue), HSC(magenta), KiDS(green).

constructed using multi frequency data (98 and 150 GHz). In order to confirm the redshift of the clusters, data from multiple wavelengths was considered, in optical/IR. The masses for cluster is estimated assuming the SZ signal-mass scaling relation and the halo mass function. For the purpose of this work, clusters that are also present in the redMaPPer catalog are used. The total number of clusters is then $1,149$, between redshifts of 0.2 to 0.7. The mass and redshift distribution of the sample is given in 2.5. The mean Redshift is 0.46 and mean mass $M_{500c} = 2.70 * 10^{14}$. The randoms catalog as given by the survey collaboration is also used.

2.4 The Photometric Galaxy Catalog

Photometric galaxies from the Year 3 results of DES[6] are used to calculate splashback radius of clusters, by using the Cluster-Galaxy cross-correlation function.

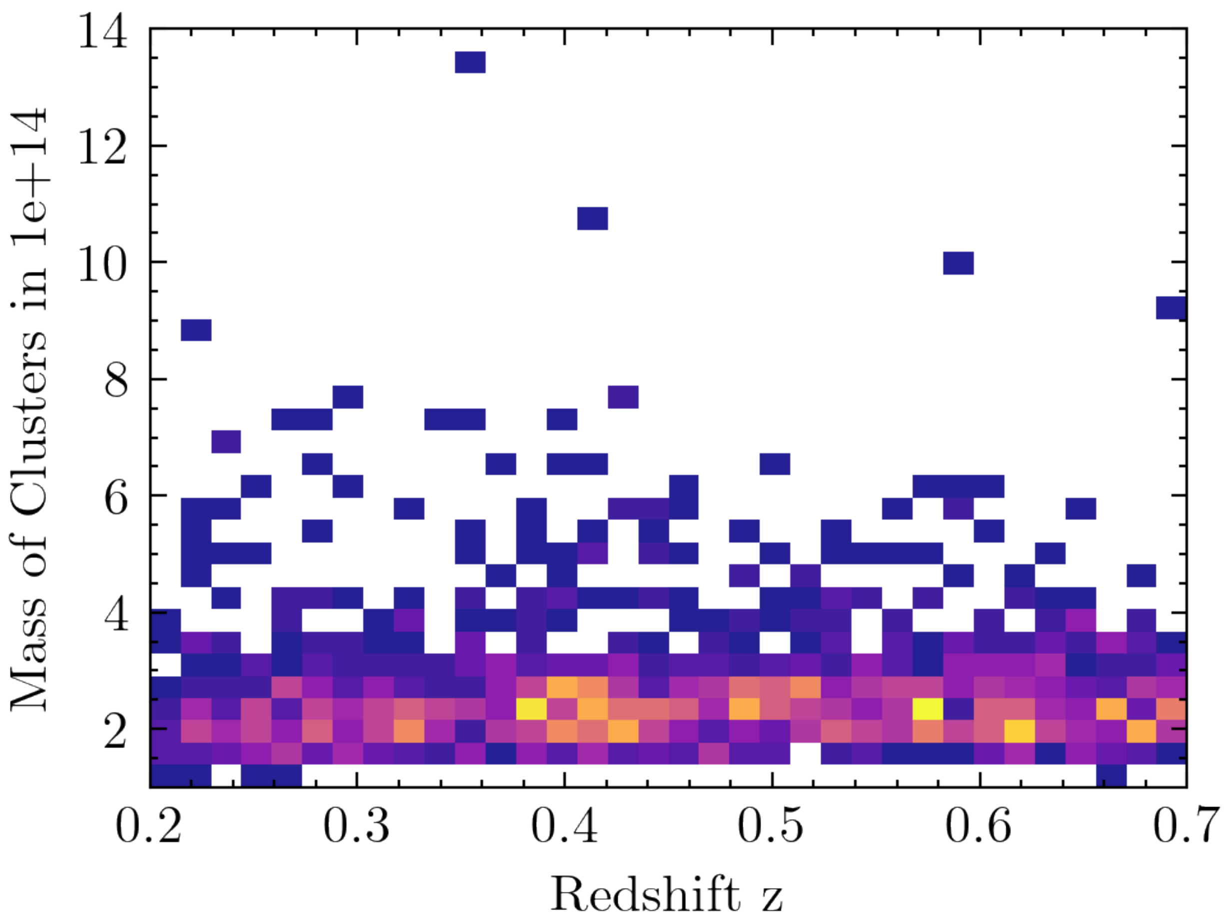

Figure 2.6: 2-D Histogram of ACT×DES-redMaPPer Clusters in Redshift-Mass bins.

Chapter 3

Measurement of Splashback

Previous chapters have dealt with the data used in this thesis and theoretical model to explain the data. Here we connect the two by going through the process of fitting data to a model. The techniques and tools discussed in this chapter are used widely in Cosmology and Astronomy. First section deals with constructing correlation function from a finite volume survey using an estimator. The second section is discussion of Bayesian inference using Monte Carlo. Finally, we put the two together in next chapter and get results.

3.1 Correlation Function

We define two-point correlation Function $\xi(\mathbf{r})$ as *the excess probability* of finding a galaxy at some distance $\mathbf{r}$ from another galaxy. Mathematically,

$$d\boldsymbol{P} =< \rho > [1 + \xi(\mathbf{r})]dV \tag{3.1}$$

$< \rho >$ is the mean number density of galaxies, and dV is the volume element at distance $\mathbf{r}$. The probability of finding a galaxy a in volume dV at some location $\mathbf{x}$ is

$$d\boldsymbol{P}_1 =< \rho(\mathbf{x}) > dV_1 =< \rho > \langle 1 + \delta(\mathbf{x})\rangle dV_1 \tag{3.2}$$

From this, the probability of finding a pair of galaxies separated by $\mathbf{r}$ is,

$$\begin{aligned}
d\boldsymbol{P}_{12} &= \langle \rho(\mathbf{x})\rho(\mathbf{x}+\mathbf{r})\rangle dV_1 dV_2 \\
&= \langle \rho\rangle^2 \langle [1+\delta(\mathbf{x})][1+\delta(\mathbf{x}+\mathbf{r})]\rangle V_1 dV_2 \\
&= \langle \rho\rangle^2 [1+\langle \delta(\mathbf{x})\rangle + \langle \delta(\mathbf{x}+\mathbf{r})\rangle + \langle \delta(\mathbf{x})\delta(\mathbf{x}+\mathbf{r})\rangle] dV_1 dV_2 \\
&= \langle \rho\rangle^2 [1+\langle \delta(\mathbf{x})\delta(\mathbf{x}+\mathbf{r})\rangle] dV_1 dV_2
\end{aligned} \tag{3.3}$$

since $\langle \delta(\mathbf{x})\rangle = \langle \delta(\mathbf{x}+\mathbf{r})\rangle = 0$. In order to get the probability of finding second galaxy after the first one, divide $d\boldsymbol{P}_{12}$ by $d\boldsymbol{P}_1$, we get,

$$d\boldsymbol{P}_2 = \langle \rho\rangle [1+\langle \delta(\mathbf{x})\delta(\mathbf{x}+\mathbf{r})\rangle] dV_2 \tag{3.4}$$

Comparing with 3.1, we can see

$$\xi(\mathbf{r}) = \langle \delta(\mathbf{x})\delta(\mathbf{x}+\mathbf{r})\rangle \tag{3.5}$$

Since Data is discrete, in order to calculate correlation function, number of galaxy pairs $dd(s)$ at some separation s, which fall within some bin Δr of the separation. But how much of this is the excess? Any random distribution of galaxies is given by *Poisson Distribution*. Therefore, the excess is in comparison to pairs of galaxies $rr(s)$ made by this process. The simplest estimator is therefore, by comparing the discrete definition to the continuum limit

$$1+\xi(s) = \frac{dd(s)}{rr(s)} \tag{3.6}$$

In order for the error to tend to zero, the number of points needs to tend to infinity. It is very difficult to increase number of data points(using telescope observation), but randoms can be scaled easily, since they can be made by using any of the numerous randoms algorithm. However, the assumption in writing the above expression is that $\langle \rho\rangle$ is the same for both, data and randoms. Therefore, the pair counts need to be scaled.

$$\begin{aligned}
DD(s) &= \frac{dd(s)}{n_d(n_d-1)/2} \\
RR(s) &= \frac{rr(s)}{n_d(n_d-1)/2}
\end{aligned} \tag{3.7}$$

The estimator is

$$1+\xi(s) = \frac{DD}{RR} \tag{3.8}$$

Since a galaxy survey surveys just a finite volume of a single realization,random error can be amplified by edge effects. In the case where the galaxies lie close to the edge of the survey these volumes are smaller as the part of the shell that falls outside the survey volume is not included. In order to account for these effects, Landay & Szalay proposed the estimator

$$\xi(s) = \frac{DD - RD - DR + RR}{RR} \tag{3.9}$$

This is the estimator used throughout this work.

3.1.1 Density profile From Data

The galaxy-cluster correlation,$w(R)$, can be correlated to the distribution of galaxies around a cluster. In order to construct the density profile, the method given in Chang et. al and Baxter et.al is followed. R here is the projected distance on the sky, and is related to the co-moving distance, $R_{comoving} = (1+z)R_{phy}$. DK14 had shown that R_{sp} scales with physical R_{200}, and since it is inversely proportional to $(1+z)$, by choosing co-moving coordinates, the dependence on redshift is factored out.

The catalog is broken into redshift bins each of width $\Delta z = 0.05$, in order to calculate mean subtracted galaxy density around a cluster. Since we observe a projection of $3-D$ universe onto a $2-D$ sky, we do not know which galaxies are in the background or in the foreground explicitly. By binning in redshift, background galaxies are removed when measuring density profile. This is done by placing an absolute magnitude cut, assuming all galaxies are at the same redshift as the cluster redshift bin. What this means is, any galaxy of absolute magnitude M_{gal} is removed if it's more that $M_{abs} - 5.0\log(h)$, with the upper limit of apparent magnitude 22.5 at $z = 0.35$ for redMaGiC catalog.

The angular correlation, $w(\theta, z_i)$ is calculated using above discussed Landay-Szalay estimator. This is converted into $w(R, z_i)$. R is the projected co-moving distance for angular separation θ. The measurement of each z bin is combined weighted with number of clusters, to get $w(R)$. To finally get density profile,

$$\Sigma_g(R) = \bar{\Sigma_g} w(R) \tag{3.10}$$

The $\bar{\Sigma_g}$ is average galaxy surface density, weighted by cluster number in each redshift bin. The covariance data is calculated by taking 100 jackknife patches using TreeCorr. The area of subregions is 7×7 square degrees, and therefore are reliable for the scales considered.

3.2 Bayesian Inference

Bayesian analysis is popular in astronomy due to several advantages over traditional methods. It provides a complete picture of parameter uncertainty, joint parameter uncertainty, and parameter relationships given the model, data, and prior assumptions. Bayesian probability intervals are appealing alternatives to point estimates with confidence intervals, which rely on the estimator's sampling distribution. Bayesian analysis easily marginalizes over nuisance parameters, incorporates measurement uncertainties through error models, and includes incomplete data such as missing and censored data. Prior knowledge about parameter values can improve the final inference by naturally including them in prior distributions. Moreover, with advancement in computer hardware and python packages(such as *emcee*[7]), Bayesian methodology has become accessible.

Let $\mathbf{d}$ represent the data vector, and $\boldsymbol{\theta}$ be the parameter vector. According to Bayes Theorem

$$P(\boldsymbol{\theta}|\mathbf{d}) = \frac{P(\mathbf{d}|\boldsymbol{\theta})P(\boldsymbol{\theta})}{P(\mathbf{d})} \tag{3.11}$$

In astronomy and astrophysics, we have the data and need to find parameter values of a model that can reproduce the data. In this paradigm, $P(\boldsymbol{\theta}|\mathbf{d})$ is what is called *posterior distribution*, $P(\boldsymbol{\theta})$ is called *prior* and $P(\mathbf{d}|\boldsymbol{\theta})$ *Likelihood function*. $P(\mathbf{d})$ is referred to as *model evidence*, and is assumed to be 1, since we assume that the model we are using is indeed the correct one. The aim is to get the posterior distribution of parameter space. Taking natural log of 3.11, we can write it

$$\ln P(\boldsymbol{\theta}|\mathbf{d}) = \ln P(\mathbf{d}|\boldsymbol{\theta}) + \ln P(\boldsymbol{\theta}) \tag{3.12}$$

Working in natural log simplifies the calculations and avoids negative values.

Priors are determined by the physical system under consideration and possible values allowed in the model. It is necessary to take priors as flat and wide as possible, such that result is not biased because of selection on priors.

Determining Likelihood function can be challenging depending on the problem. Most often, it is taken to be a product of independent and identically distributed Gaussian random variable with known variance. This can be written as,

$$\ln P(\mathbf{d}|\boldsymbol{\theta}) = \ln \mathcal{L}[\vec{d}|\vec{m}(\vec{\theta})] = -\frac{1}{2}[\vec{d} - \vec{m}(\vec{\theta})]^T \boldsymbol{C^{-1}}[\vec{d} - \vec{m}(\vec{\theta})] \tag{3.13}$$

Here $\vec{m}(\vec{\theta})$ is the model evaluated for a given parameter vector.
In order to sample the posterior distribution, given priors and likelihood, Markov Chain Monte Carlo is used. One such algorithm to do the same is discussed in next section. The priors used here are the same as in [3].

Parameters	**Priors**
ρ_s	$[0.1, 10]g/cm^3$
r_s	$[0.1, 5]h^{-1}Mpc$
r_t	$[0.1, 5]h^{-1}Mpc$
$\log(\alpha)$	$\log(0.19) \pm 0.2$
$\log(\beta)$	$\log(6) \pm 0.2$
$\log(\gamma)$	$\log(4) \pm 0.2$
ρ_0	$[0.1, 10]g/cm^3$
s_e	[1,10]

Table 3.1: The ranges in square brackets are uniform priors, and for the others it is a normal distribution with mean and error.

3.3 Introduction to Emcee

The posterior distribution can be multi-dimensional,asymmetric and with multiple modes. In order to correctly estimate the distribution, Monte Carlo sampling becomes very useful. In Metropolis-Hastings algorithm, one random walker traverses the parameter space. Over the years, many more sampling variations on this principle have emerged. The one used in

this project was developed by David and ForMcKay. It has multiple walkers that parallely explore the parameter space.
A walker is drawn at random, $\theta_j (j \neq k)$ and it's position is updated by

$$\theta_k(t) \rightarrow \theta^{'} = \theta_j + Z[\theta_k(t) - \theta_j] \tag{3.14}$$

where Z is a random variable. The acceptance probability of the step is

$$q = min\left(1, Z^{-1} \frac{P(\theta^{'})}{P(\theta_k(t))}\right) \tag{3.15}$$

This process is repeated for all walkers, iterated over many steps, to approximate the posterior as accurately as possible.

Chapter 4

Results and Discussion

The first goal of the project was to build the code that can detect splashback radius around cluster mass halos. Figure4.1a shows the density profile and splashback radius 4.1bs around redMaPPer clusters. The value is $1.27 \pm 0.03h^{-1}Mpc$. This is in good agreement with the value from [3], who used similar selection cuts on the catalog. 4.2b also shows splashback radius of ACT clusters, which was first calculated in cite. The splashback obtained is $1.99 \pm 0.04h^{-1}Mpc$, again in agreement with the value previously inferred. Therefore, the code can reliably detect splashback radius.

In figure4.4a, the brightest one percentile of the redMaGiC sample is selected. This is to select for galaxies that are very likely cluster centres, since brightest galaxies reside in heaviest halos. Although there is scatter in this relationship,it selects for largest halos in the catalog. The splashback radius for these galaxies turns out to be $1.30 \pm 0.03h^{-1}Mpc$. This is very close to the value of redMaPPer clusters. It's possible that the brightest clusters in redMaGiC are also present in the redMaPPer catalog. In order to check for this, cross correlation between the two catalog was done, and the number of galaxies that were found to be within $1h^{-1}Mpc$ was 3%. Therefore, these are different galaxies. Since splashback radius is correlated with mass of halos, this gives merit to the statement that brightest galaxies are in largest halos.

In order to go down the mass range, galaxies in the lower brightness were selected. 4.4b shows the density profile as well as logarithmic slope of galaxies in second bin, followed by fifth and tenth bin. Each bin has 3699 number of galaxies. As can be seen, the brightest galaxies have largest splashback radius, as well the most clearly defined dip in the slope

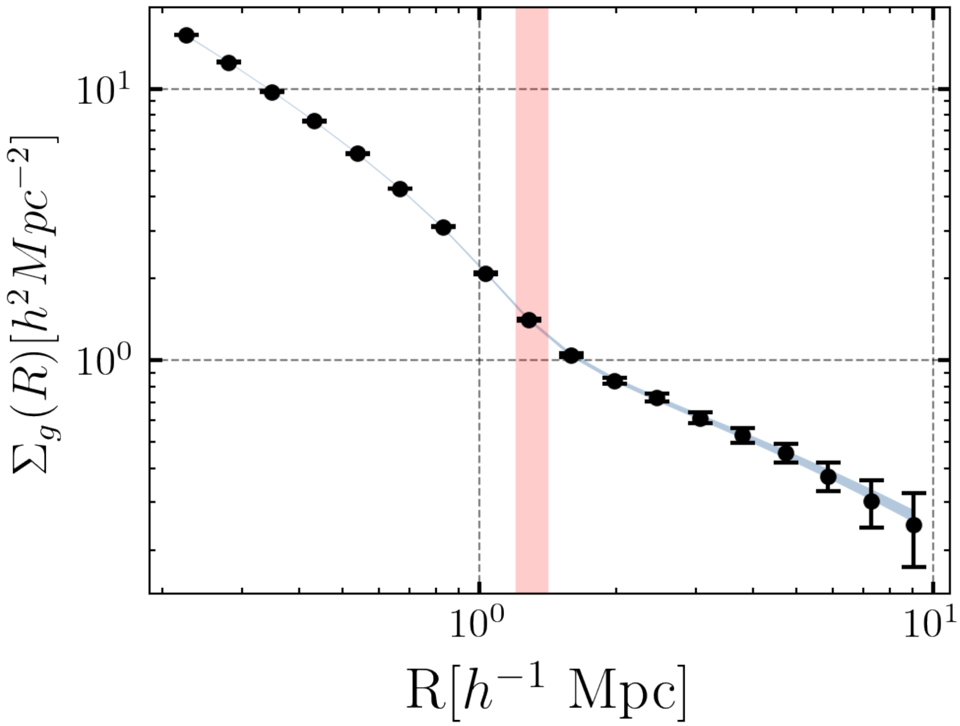

(a) Density profile of redMaPPer clusters for $0.2 < z < 0.7$

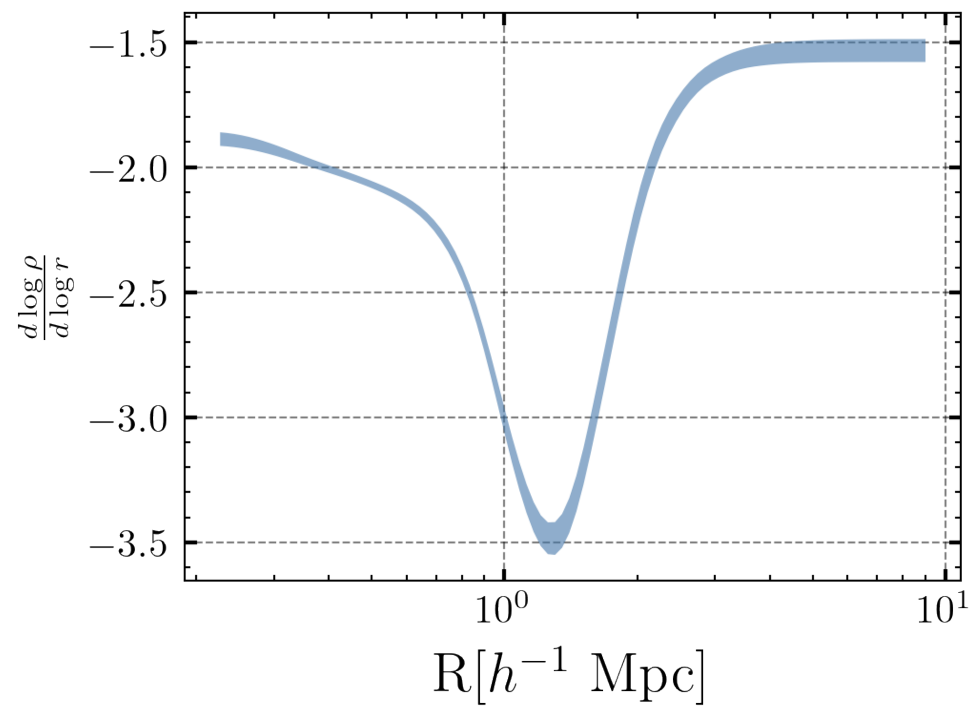

(b) Slope profile of redMaPPer clusters for $0.2 < z < 0.7$

Figure 4.1: redMaPPer Clusters

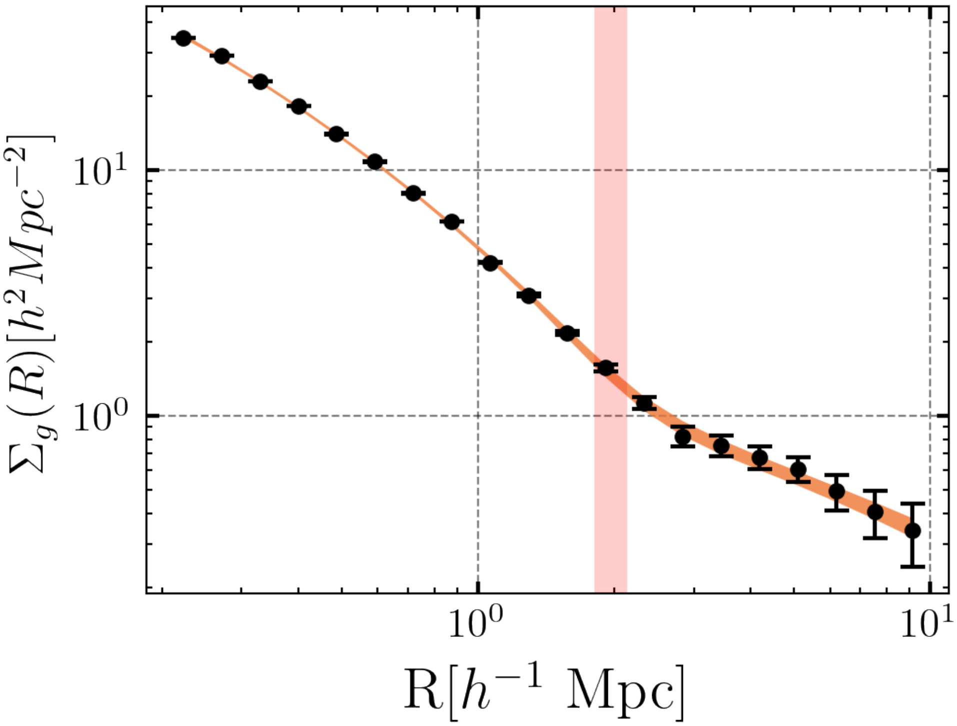

(a) Density profile of ACT clusters also present in the DES for $0.2 < z < 0.7$

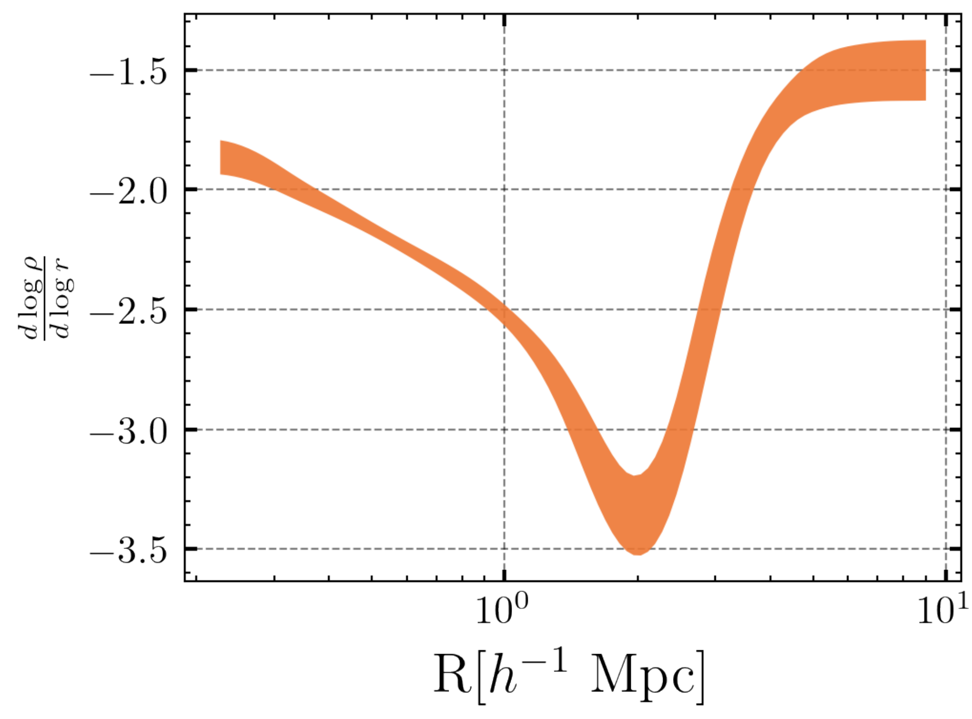

(b) Slope profile of ACT clusters also present in DES for $0.2 < z < 0.7$

Figure 4.2: ACT results

profile. As we move down the order, the shallowness and the size also decrease. However, the fifth percentile of galaxies seem to have smaller and shallower profile than that of less bright, tenth percentile binned galaxies. This can be due the the fit not able to fully capture the profile around halo boundary because of two halo term. For lower mass halos, their environments effect the profile much more prominently,since their potential wells are shallower compared to clusters. Therefore, we choose different environments, based on density cuts.
In order to construct the a density map, the same procedure is followed as done in [13]. The sky positions are converted into pixel coordinates using HEALPY package, and the number of galaxies counted in each pixel. To get density field, this number is divided against the area of each pixel. In order to get density contrast, the background average density is subtracted from density of each pixel,and is normalised against average density. This is done in each redshift bin. Fig shows the histogram of density contrast in few bins that are used. We select for the most under dense and most dense regions, in twenty five percentile bins.

4.5a shows the density and 4.5b slope profile for top two percentile brightest galaxies, when different density environments are taken. Galaxies in the most dense environments have the shallowest profile, and also the smallest. One possible reason for slightly smaller radius could be the higher accretion rates. Since there is more matter in dense environments, more of it can be accreted. Diemer and Kratsov in their work showed that higher accretion rates lead to smaller splashback radius. The shallowness of the slope is a statement of how fast the density profile steepens near the splashback radius. With more matter around, this steeping becomes less prominent.

4.6a shows the profile for next brightness bin. Here the profiles are also ranked within each density bin, to make sure similar mass halos are selected throughout. From the slope profiles,4.6b the least dense regions have the smallest radius, but the most deep profile. Here, we believe the fit in most dense environments is not fitting just to DK profile, but to two halo terms as well. There is also movement of the location of the splashback radius in different environments. The magnitude is same, but it's possible that because of density cuts, a bias in the mass of halos is introduced.

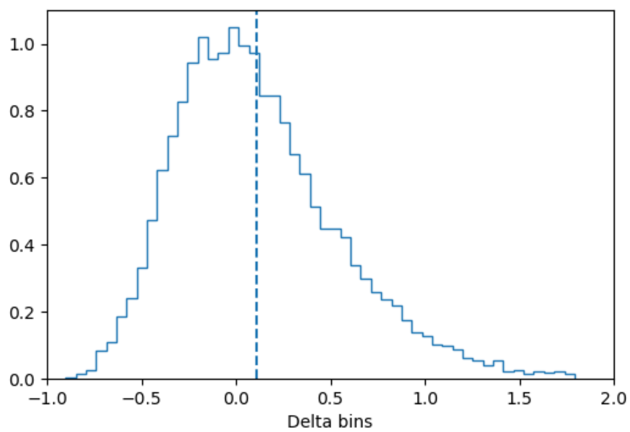

(a) Delta for $0.15 < z < 0.2$

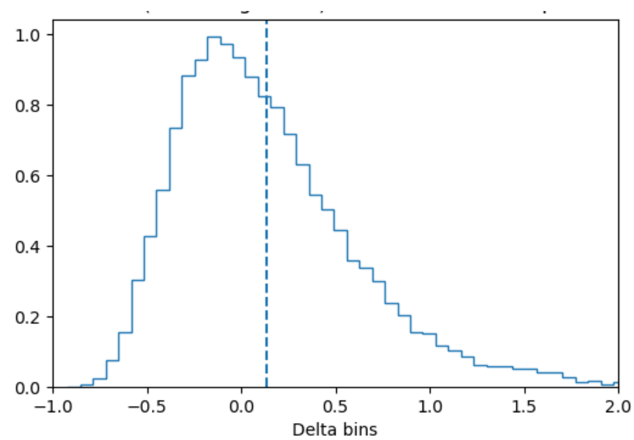

(b) Delta for $0.2 < z < 0.25$

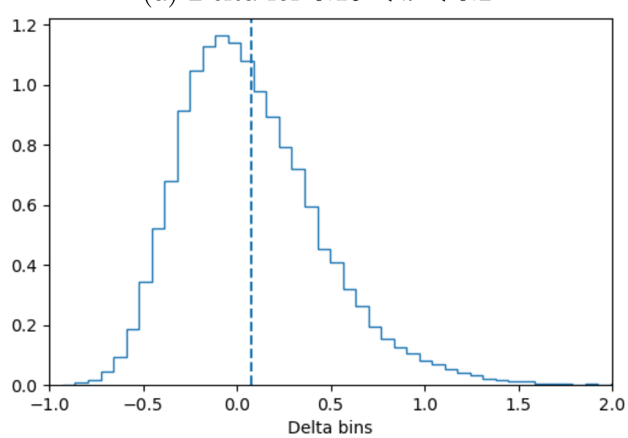

(c) Delta for $0.25 < z < 0.3$

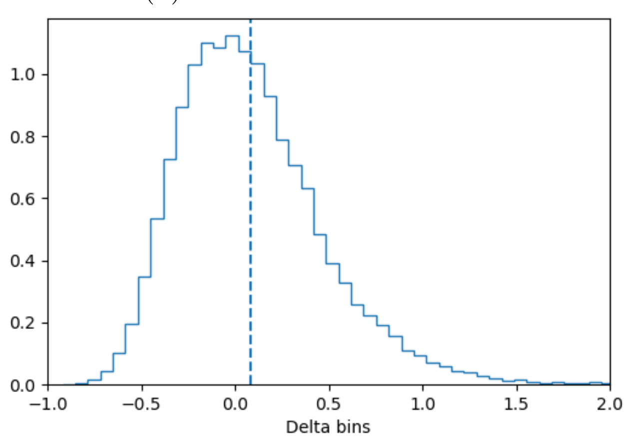

(d) Delta for $0.3 < z < 0.35$

Figure 4.3: Distribution of density contrast across redshift

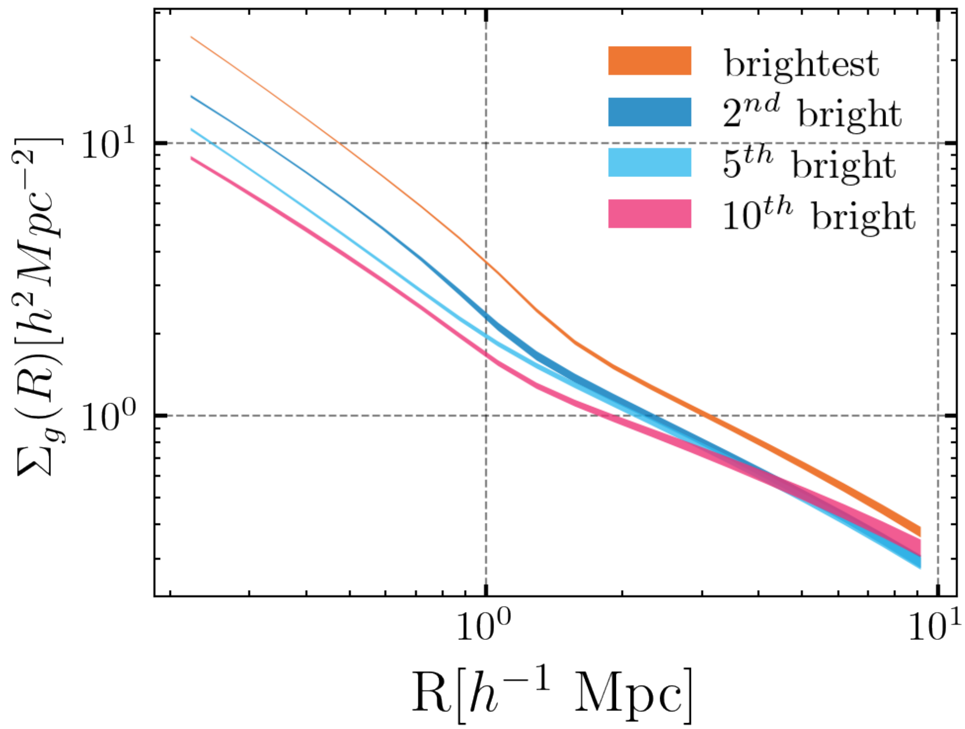

(a) Density profile for redMagic galaxies in first, second, fifth and tenth brightness percentile bins.

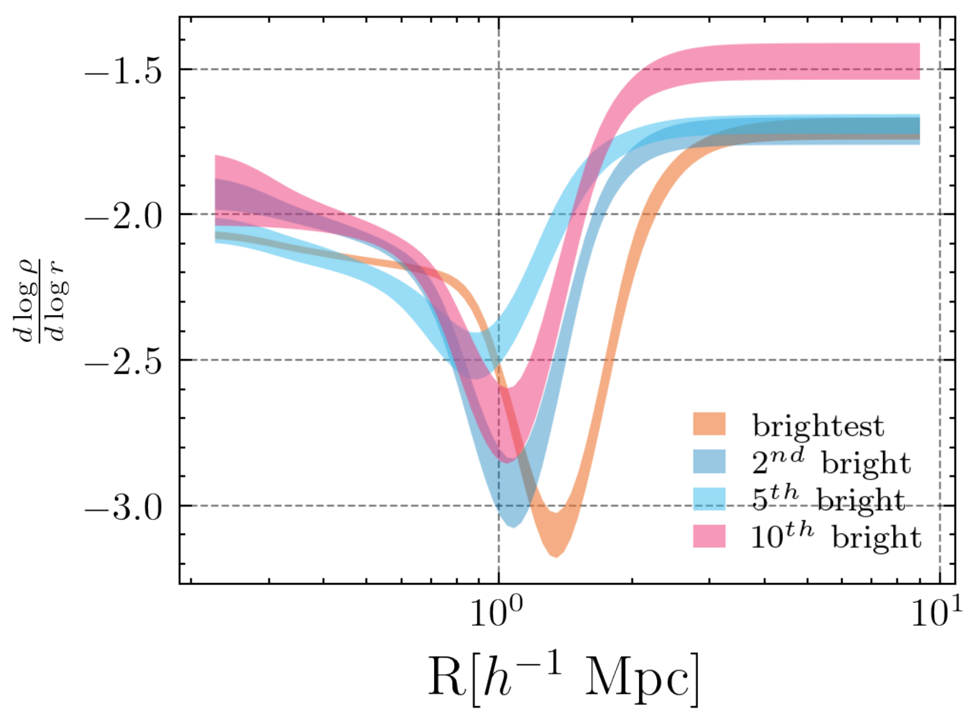

(b) Logarithmic slope for redMagic galaxies in first, second, fifth and tenth brightness percentile bins.

Figure 4.4: redMaGiC across magnitude bins

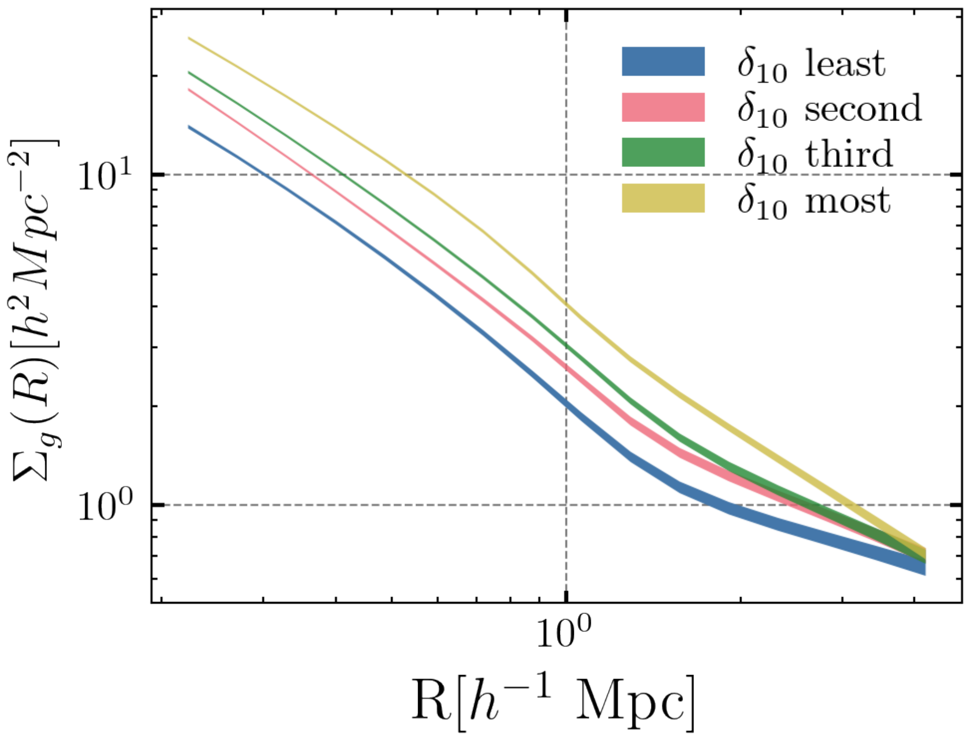

(a) Density profile for brightest two percentile redMagic galaxies with different density cuts.

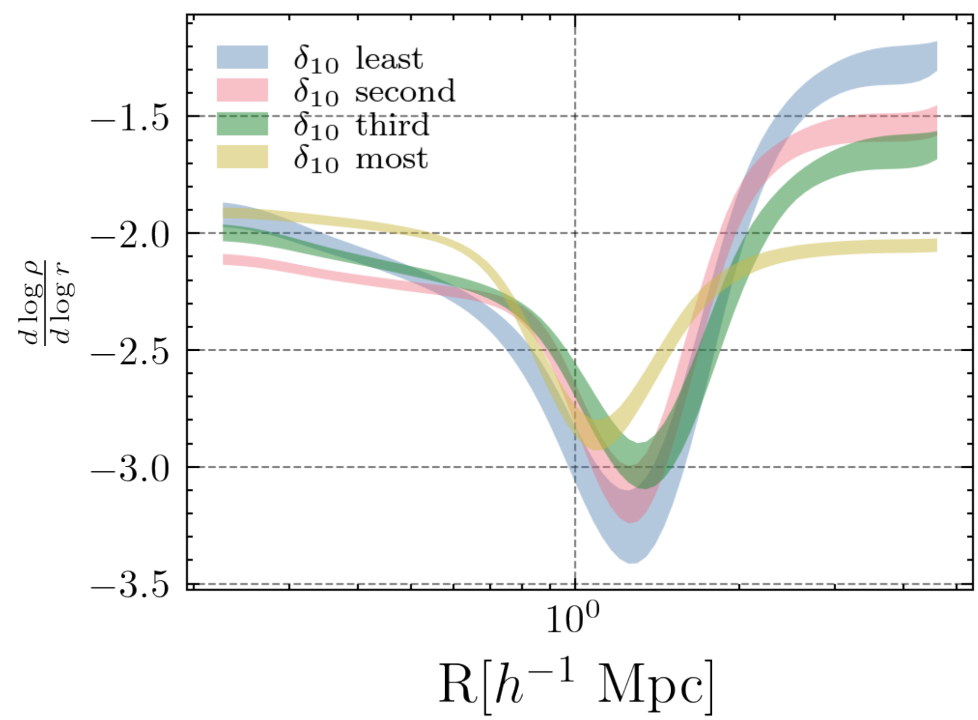

(b) Logarithmic slope for brightest two percentile redMagic galaxies with different density cuts.

Figure 4.5: Brightest redMaGiC in different environments

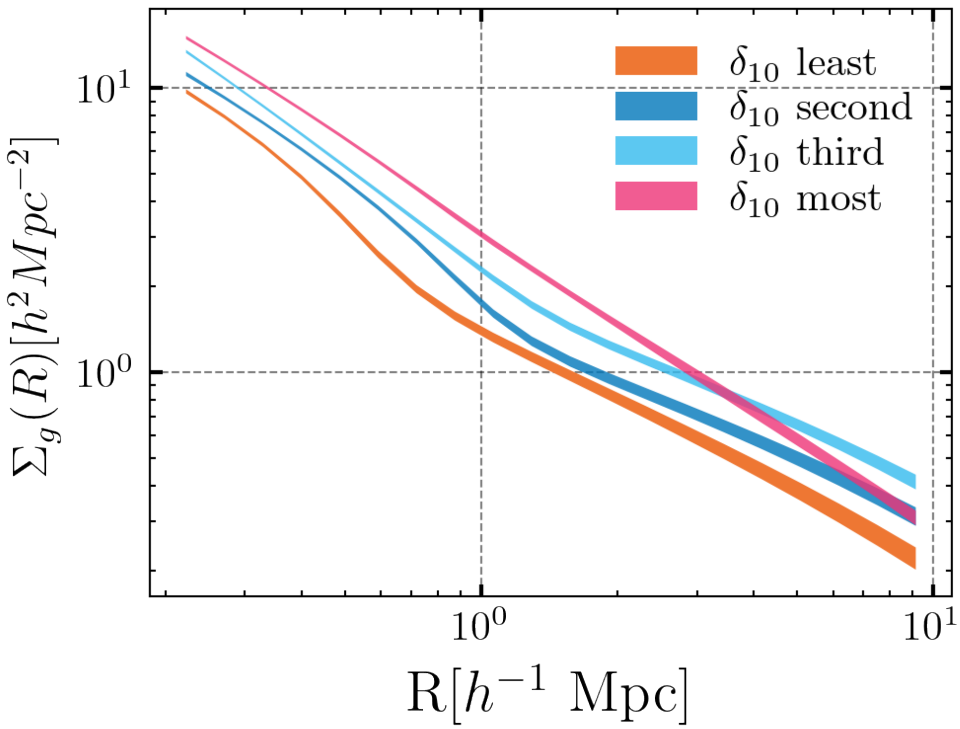

(a) Density profile for second brightest two percentile redMagic galaxies with different density cuts.

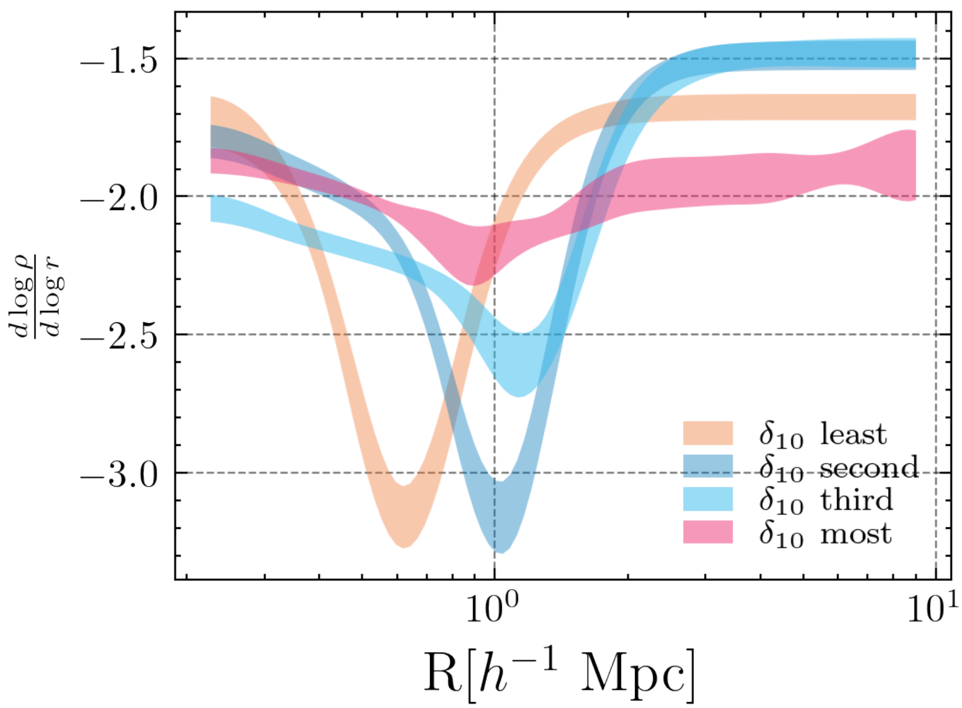

(b) Logarithmic slope for second brightest two percentile redMagic galaxies with different density cuts.

Figure 4.6: redMaGiC in different environments

Chapter 5

Conclusion

We have looked at the density profile of clusters and galaxies and inferred the splashback radius of these objects. The density of groups is also studied in different environments of the universe. There still remain open questions as about how the environment affects splashback, and the goal to study halos of lower mass further. Exactly which of effects, such as tidal disruption, dynamical friction or star formation quenching and how much they affect the halo profile is to be studied, by comparing data and measurements, such as done in this work, to simulations. In dealing with redMaGic galaxies, there is very less information about the mass of halos, and one future direction of this work is to study the matter density profile using weak lensing analysis. It can also help in characterising mass bias. This analysis can also be done on ACT clusters, which have their mass and R_{200} characterised.

In their 2014 paper, Diemer and Kravtsov, followed by others have shown that splashback radius normalised by r_{200} is a function of accretion rates. Accretion rate of halos is difficult to obtain using direct measurement, and understanding splashback radius can help also constrain accretion rates for different size of halos across redshift. Splashback can also be a probe to study Self-Interacting Dark Matter Models(SIDM), since the density profiles are sensitive to type of dark matter. Data from future surveys, like LSST and Euclid, which are expected to observe fainter galaxies, will be helpful in measuring the density profiles of even lower mass galaxies than groups.

Much remains in the study of Splashback radius as it is a very new avenue of characterising halo boundary, and this work adds to the growing literature around this topic.

Bibliography

[1] Cosmology by David Tong.

[2] S. Adhikari, N. Dalal, and R. T. Chamberlain. Splashback in accreting dark matter halos. *Journal of Cosmology and Astroparticle Physics*, 2014(11):019–019, Nov. 2014.

[3] C. Chang, E. Baxter, B. Jain, C. Sánchez, S. Adhikari, T. N. Varga, Y. Fang, E. Rozo, E. S. Rykoff, A. Kravtsov, D. Gruen, E. M. Huff, M. Jarvis, A. G. Kim, J. Prat, N. MacCrann, T. McClintock, A. Palmese, D. Rapetti, R. P. Rollins, S. Samuroff, E. Sheldon, M. A. Troxel, R. H. Wechsler, Y. Zhang, J. Zuntz, T. M. C. Abbott, F. B. Abdalla, S. Allam, J. Annis, K. Bechtol, A. Benoit-Lévy, G. M. Bernstein, D. Brooks, E. Buckley-Geer, A. C. Rosell, M. C. Kind, J. Carretero, C. B. D'Andrea, L. N. da, C. Davis, S. Desai, H. T. Diehl, J. P. Dietrich, A. Drlica-Wagner, T. F. Eifler, B. Flaugher, P. Fosalba, J. Frieman, J. García-Bellido, E. Gaztanaga, D. W. Gerdes, R. A. Gruendl, J. Gschwend, G. Gutierrez, K. Honscheid, D. J. James, T. Jeltema, E. Krause, K. Kuehn, O. Lahav, M. Lima, M. March, J. L. Marshall, P. Martini, P. Melchior, F. Menanteau, R. Miquel, J. J. Mohr, B. Nord, R. L. C. Ogando, A. A. Plazas, E. Sanchez, V. Scarpine, R. Schindler, M. Schubnell, I. Sevilla-Noarbe, R. C. Smith, M. Smith, M. Soares-Santos, F. Sobreira, E. Suchyta, M. E. C. Swanson, G. Tarle, and J. Weller. The Splashback Feature around DES Galaxy Clusters: Galaxy Density and Weak Lensing Profiles. *The Astrophysical Journal*, 864(1):83, Aug. 2018. arXiv:1710.06808 [astro-ph].

[4] B. Diemer and A. V. Kravtsov. DEPENDENCE OF THE OUTER DENSITY PROFILES OF HALOS ON THEIR MASS ACCRETION RATE. *The Astrophysical Journal*, 789(1):1, June 2014.

[5] S. Dodelson and F. Schmidt. *Modern cosmology.* Academic Press, an imprint of Elsevier, London, United Kingdom ; San Diego, CA, second edition edition, 2021. OCLC: on1180066787.

[6] A. Drlica-Wagner, I. Sevilla-Noarbe, E. S. Rykoff, R. A. Gruendl, B. Yanny, D. L. Tucker, B. Hoyle, A. C. Rosell, G. M. Bernstein, K. Bechtol, M. R. Becker, A. Benoit-Levy, E. Bertin, M. C. Kind, C. Davis, J. de Vicente, H. T. Diehl, D. Gruen, W. G. Hartley, B. Leistedt, T. S. Li, J. L. Marshall, E. Neilsen, M. M. Rau, E. Sheldon, J. Smith, M. A. Troxel, S. Wyatt, Y. Zhang, T. M. C. Abbott, F. B. Abdalla, S. Allam,

M. Banerji, D. Brooks, E. Buckley-Geer, D. L. Burke, D. Capozzi, J. Carretero, C. E. Cunha, C. B. D'Andrea, L. N. da Costa, D. L. DePoy, S. Desai, J. P. Dietrich, P. Doel, A. E. Evrard, A. F. Neto, B. Flaugher, P. Fosalba, J. Frieman, J. Garcia-Bellido, D. W. Gerdes, T. Giannantonio, J. Gschwend, G. Gutierrez, K. Honscheid, D. J. James, T. Jeltema, K. Kuehn, S. Kuhlmann, N. Kuropatkin, O. Lahav, M. Lima, H. Lin, M. A. G. Maia, P. Martini, R. G. McMahon, P. Melchior, F. Menanteau, R. Miquel, R. C. Nichol, R. L. C. Ogando, A. A. Plazas, A. K. Romer, A. Roodman, E. Sanchez, V. Scarpine, R. Schindler, M. Schubnell, M. Smith, R. C. Smith, M. Soares-Santos, F. Sobreira, E. Suchyta, G. Tarle, V. Vikram, A. R. Walker, R. H. Wechsler, and J. Zuntz. Dark Energy Survey Year 1 Results: Photometric Data Set for Cosmology. *The Astrophysical Journal Supplement Series*, 235(2):33, Apr. 2018. arXiv:1708.01531 [astro-ph].

[7] D. Foreman-Mackey, D. W. Hogg, D. Lang, and J. Goodman. emcee: The MCMC Hammer. *Publications of the Astronomical Society of the Pacific*, 125(925):306–312, Mar. 2013. arXiv:1202.3665 [astro-ph, physics:physics, stat].

[8] M. Hilton, C. Sifón, S. Naess, M. Madhavacheril, M. Oguri, E. Rozo, E. Rykoff, T. M. C. Abbott, S. Adhikari, M. Aguena, S. Aiola, S. Allam, S. Amodeo, A. Amon, J. Annis, B. Ansarinejad, C. Aros-Bunster, J. E. Austermann, S. Avila, D. Bacon, N. Battaglia, J. A. Beall, D. T. Becker, G. M. Bernstein, E. Bertin, T. Bhandarkar, S. Bhargava, J. R. Bond, D. Brooks, D. L. Burke, E. Calabrese, M. Carrasco Kind, J. Carretero, S. K. Choi, A. Choi, C. Conselice, L. N. D. Costa, M. Costanzi, D. Crichton, K. T. Crowley, R. Dünner, E. V. Denison, M. J. Devlin, S. R. Dicker, H. T. Diehl, J. P. Dietrich, P. Doel, S. M. Duff, A. J. Duivenvoorden, J. Dunkley, S. Everett, S. Ferraro, I. Ferrero, A. Ferté, B. Flaugher, J. Frieman, P. A. Gallardo, J. García-Bellido, E. Gaztanaga, D. W. Gerdes, P. Giles, J. E. Golec, M. B. Gralla, S. Grandis, D. Gruen, R. A. Gruendl, J. Gschwend, G. Gutierrez, D. Han, W. G. Hartley, M. Hasselfield, J. C. Hill, G. C. Hilton, A. D. Hincks, S. R. Hinton, S.-P. P. Ho, K. Honscheid, B. Hoyle, J. Hubmayr, K. M. Huffenberger, J. P. Hughes, A. T. Jaelani, B. Jain, D. J. James, T. Jeltema, S. Kent, K. Knowles, B. J. Koopman, K. Kuehn, O. Lahav, M. Lima, Y.-T. Lin, M. Lokken, S. I. Loubser, N. MacCrann, M. A. G. Maia, T. A. Marriage, J. Martin, J. McMahon, P. Melchior, F. Menanteau, R. Miquel, H. Miyatake, K. Moodley, R. Morgan, T. Mroczkowski, F. Nati, L. B. Newburgh, M. D. Niemack, A. J. Nishizawa, R. L. C. Ogando, J. Orlowski-Scherer, L. A. Page, A. Palmese, B. Partridge, F. Paz-Chinchón, P. Phakathi, A. A. Plazas, N. C. Robertson, A. K. Romer, A. C. Rosell, M. Salatino, E. Sanchez, E. Schaan, A. Schillaci, N. Sehgal, S. Serrano, T. Shin, S. M. Simon, M. Smith, M. Soares-Santos, D. N. Spergel, S. T. Staggs, E. R. Storer, E. Suchyta, M. E. C. Swanson, G. Tarle, D. Thomas, C. To, H. Trac, J. N. Ullom, L. R. Vale, J. V. Lanen, E. M. Vavagiakis, J. D. Vicente, R. D. Wilkinson, E. J. Wollack, Z. Xu, and Y. Zhang. The Atacama Cosmology Telescope: A Catalog of >4000 Sunyaev–Zel'dovich Galaxy Clusters. *The Astrophysical Journal Supplement Series*, 253(1):3, Mar. 2021.

[9] S. More, H. Miyatake, M. Takada, B. Diemer, A. V. Kravtsov, N. K. Dalal, A. More, R. Murata, R. Mandelbaum, E. Rozo, E. S. Rykoff, M. Oguri, and D. N. Spergel.

Detection of the Splashback Radius and Halo Assembly bias of Massive Galaxy Clusters. *The Astrophysical Journal*, 825(1):39, June 2016. arXiv:1601.06063 [astro-ph].

[10] E. Rozo, E. S. Rykoff, A. Abate, C. Bonnett, M. Crocce, C. Davis, B. Hoyle, B. Leistedt, H. V. Peiris, R. H. Wechsler, T. Abbott, F. B. Abdalla, M. Banerji, A. H. Bauer, A. Benoit-Lévy, G. M. Bernstein, E. Bertin, D. Brooks, E. Buckley-Geer, D. L. Burke, D. Capozzi, A. C. Rosell, D. Carollo, M. C. Kind, J. Carretero, F. J. Castander, M. J. Childress, C. E. Cunha, C. B. D'Andrea, T. Davis, D. L. DePoy, S. Desai, H. T. Diehl, J. P. Dietrich, P. Doel, T. F. Eifler, A. E. Evrard, A. F. Neto, B. Flaugher, P. Fosalba, J. Frieman, E. Gaztanaga, D. W. Gerdes, K. Glazebrook, D. Gruen, R. A. Gruendl, K. Honscheid, D. J. James, M. Jarvis, A. G. Kim, K. Kuehn, N. Kuropatkin, O. Lahav, C. Lidman, M. Lima, M. A. G. Maia, M. March, P. Martini, P. Melchior, C. J. Miller, R. Miquel, J. J. Mohr, R. C. Nichol, B. Nord, C. R. O'Neill, R. Ogando, A. A. Plazas, A. K. Romer, A. Roodman, M. Sako, E. Sanchez, B. Santiago, M. Schubnell, I. Sevilla-Noarbe, R. C. Smith, M. Soares-Santos, F. Sobreira, E. Suchyta, M. E. C. Swanson, J. Thaler, D. Thomas, S. Uddin, V. Vikram, A. R. Walker, W. Wester, Y. Zhang, and L. N. Da Costa. redMaGiC: selecting luminous red galaxies from the DES Science Verification data. *Monthly Notices of the Royal Astronomical Society*, 461(2):1431–1450, Sept. 2016.

[11] E. S. Rykoff, E. Rozo, M. T. Busha, C. E. Cunha, A. Finoguenov, A. Evrard, J. Hao, B. P. Koester, A. Leauthaud, B. Nord, M. Pierre, R. Reddick, T. Sadibekova, E. S. Sheldon, and R. H. Wechsler. redMaPPer. I. ALGORITHM AND SDSS DR8 CATALOG. *The Astrophysical Journal*, 785(2):104, Apr. 2014.

[12] T. Shin, S. Adhikari, E. J. Baxter, C. Chang, B. Jain, N. Battaglia, L. Bleem, S. Bocquet, J. DeRose, D. Gruen, M. Hilton, A. Kravtsov, T. McClintock, E. Rozo, E. S. Rykoff, T. N. Varga, R. H. Wechsler, H. Wu, Z. Zhang, S. Aiola, S. Allam, K. Bechtol, B. A. Benson, E. Bertin, J. R. Bond, M. Brodwin, D. Brooks, E. Buckley-Geer, D. L. Burke, J. E. Carlstrom, A. Carnero Rosell, M. Carrasco Kind, J. Carretero, F. J. Castander, S. K. Choi, C. E. Cunha, T. M. Crawford, L. N. da Costa, J. De Vicente, S. Desai, M. J. Devlin, J. P. Dietrich, P. Doel, J. Dunkley, T. F. Eifler, A. E. Evrard, B. Flaugher, P. Fosalba, P. A. Gallardo, J. García-Bellido, E. Gaztanaga, D. W. Gerdes, M. Gralla, R. A. Gruendl, J. Gschwend, N. Gupta, G. Gutierrez, W. G. Hartley, J. C. Hill, S. P. Ho, D. L. Hollowood, K. Honscheid, B. Hoyle, K. Huffenberger, J. P. Hughes, D. J. James, T. Jeltema, A. G. Kim, E. Krause, K. Kuehn, O. Lahav, M. Lima, M. S. Madhavacheril, M. A. G. Maia, J. L. Marshall, L. Maurin, J. McMahon, F. Menanteau, C. J. Miller, R. Miquel, J. J. Mohr, S. Naess, F. Nati, L. Newburgh, M. D. Niemack, R. L. C. Ogando, L. A. Page, B. Partridge, S. Patil, A. A. Plazas, D. Rapetti, C. L. Reichardt, A. K. Romer, E. Sanchez, V. Scarpine, R. Schindler, S. Serrano, M. Smith, R. C. Smith, M. Soares-Santos, F. Sobreira, S. T. Staggs, A. Stark, G. Stein, E. Suchyta, M. E. C. Swanson, G. Tarle, D. Thomas, A. van Engelen, E. J. Wollack, and Z. Xu. Measurement of the splashback feature around SZ-selected Galaxy clusters with DES,

SPT, and ACT. *Monthly Notices of the Royal Astronomical Society*, 487(2):2900–2918, Aug. 2019.

[13] C. Sánchez, J. Clampitt, A. Kovacs, B. Jain, J. García-Bellido, S. Nadathur, D. Gruen, N. Hamaus, D. Huterer, P. Vielzeuf, A. Amara, C. Bonnett, J. DeRose, W. G. Hartley, M. Jarvis, O. Lahav, R. Miquel, E. Rozo, E. S. Rykoff, E. Sheldon, R. H. Wechsler, J. Zuntz, T. M. C. Abbott, F. B. Abdalla, J. Annis, A. Benoit-Lévy, G. M. Bernstein, R. A. Bernstein, E. Bertin, D. Brooks, E. Buckley-Geer, A. C. Rosell, M. C. Kind, J. Carretero, M. Crocce, C. E. Cunha, C. B. D'Andrea, L. N. Da Costa, S. Desai, H. T. Diehl, J. P. Dietrich, P. Doel, A. E. Evrard, A. F. Neto, B. Flaugher, P. Fosalba, J. Frieman, E. Gaztanaga, R. A. Gruendl, G. Gutierrez, K. Honscheid, D. J. James, E. Krause, K. Kuehn, M. Lima, M. A. G. Maia, J. L. Marshall, P. Melchior, A. A. Plazas, K. Reil, A. K. Romer, E. Sanchez, M. Schubnell, I. Sevilla-Noarbe, R. C. Smith, M. Soares-Santos, F. Sobreira, E. Suchyta, G. Tarle, D. Thomas, A. R. Walker, J. Weller, and The DES Collaboration. Cosmic voids and void lensing in the Dark Energy Survey Science Verification data. *Monthly Notices of the Royal Astronomical Society*, 465(1):746–759, Feb. 2017.

[14] The Dark Energy Survey Collaboration. The Dark Energy Survey, Oct. 2005. arXiv:astro-ph/0510346.

[15] M. Vargas-Magaña, J. E. Bautista, J.-C. Hamilton, N. G. Busca, Aubourg, A. Labatie, J.-M. L. Goff, S. Escoffier, M. Manera, C. K. McBride, D. P. Schneider, and C. N. A. Willmer. An optimized correlation function estimator for galaxy surveys. *Astronomy & Astrophysics*, 554:A131, June 2013. arXiv:1211.6211 [astro-ph].